Global acceleration in rates of vegetation change over the past 18,000 years

Ondřej Mottl[1*†], Suzette G.A. Flantua[2*†], Kuber P. Bhatta[1], Vivian A. Felde[2], Thomas Giesecke[3],

Simon Goring[4,5], Eric C. Grimm[6‡], Simon Haberle[7,8], Henry Hooghiemstra[9], Sarah Ivory[10], Petr

Kuneš[11], Steffen Wolters[12], Alistair W. R. Seddon[2], John W. Williams[4,5]

Affiliations

1. Department of Biological Sciences, University of Bergen, PO Box 7803, N-5020 Bergen, Norway

2. Department of Biological Sciences and Bjerknes Centre for Climate Research, University of

Bergen, PO Box 7803, N-5020 Bergen, Norway.

3. Department of Physical Geography, Utrecht University, P.O. Box 80115, 3508 TC Utrecht, The

Netherlands.

4. Department of Geography, University of Wisconsin-Madison, Madison, WI, USA

5. Center for Climatic Research, University of Wisconsin-Madison, Madison, WI, USA

6. Department of Earth and Environmental Sciences, University of Minnesota, Minneapolis,

Minnesota 55455, USA

7. Department of Archaeology and Natural History, Australian National University, Canberra, ACT

2601, Australia.

8. Australian Research Council Centre of Excellence in Australian Biodiversity and Heritage,

Australian National University, Canberra, ACT 2601, Australia

9. Department of Ecosystem and Landscape Dynamics, University of Amsterdam, Science Park 904,

1098 XH, Amsterdam, the Netherlands

10. Department of Geosciences and the Earth and Environmental Systems Institute (EESI), Penn State

University, University Park, PA 16801, USA

11. Department of Botany, Faculty of Science, Charles University, Czech Republic

27   12. Lower Saxony Institute for Historical Coastal Research, Wilhelmshaven, Germany.

28   †Equal contribution. ‡ Deceased.

29

30   *Corresponding authors: Ondrej Mottl (ondrej.mottl@gmail.com), Suzette Flantua

31   (s.g.a.flantua@gmail.com)

32

33   **One sentence summary:** A compilation of over 1000 fossil pollen sequences shows that global

34   vegetation change accelerated several thousand years ago.

35

36   **Abstract**

37   Global vegetation over the last 18,000 years was transformed first by the climate changes

38   accompanying the last deglaciation and again by increasing human pressures, but the magnitude and

39   patterns of rates of vegetation change are poorly understood globally. Using a compilation of 1181

40   fossil pollen sequences and new statistical methods, we detect a worldwide acceleration in rates of

41   vegetation compositional change beginning between 4.6 and 2.9 ka that is globally unprecedented over

42   the last 18,000 years in magnitude and extent. Late Holocene rates of change equal or exceed deglacial

43   rates for all continents, suggesting that the scale of human impacts on terrestrial ecosystems exceeds

44   even the climate-driven transformations of the last deglaciation. The acceleration of biodiversity

45   change demonstrated in last-century ecological datasets began millennia ago.

46

47   **Main text**

48   One of the clearest forms of biodiversity change during the past century has been the increased rates of

49   species turnover across the marine and terrestrial biosphere (*1–3*). Today, over 75% of the Earth's ice-

50   free land surface has been altered by human land use (*4*), with profound effects on the composition

51   and functioning of ecosystems. Globally, extinction rates are increasing (*5*), although trends in local

52   species richness are ambiguous (*6*).

53   These increased rates of species turnover, as signified by local and regional changes in

54   community composition, are embedded within a longer-term context in which humanity's footprint

55 has steadily grown since humans first began to alter landscapes for food, energy, and other resources.

56 Hominid use of fire began at least 700,000 years ago (*7*), low-intensity but extensive agricultural land

57 use began ca. 8000 years ago, while intensive agricultural land use expanded after 6000 years ago (*8*)

58 (**Fig. 1B**). Detectable human imprints on vegetation began thousands of years ago (e.g. *9*, *10*), and the

59 composition and carbon sequestration of many contemporary ecosystems remain profoundly

60 influenced by legacies of past centuries to millennia of anthropogenic land use (e.g. *11*). Nonetheless,

61 there remains a major knowledge and scale gap between contemporary studies of global biodiversity

62 trends of the last century (*2*) and studies examining early anthropogenic effects on ecosystems.

63 Observational syntheses of global biodiversity trends are limited to the past several centuries, while

64 macroscale syntheses of vegetation changes from fossil pollen data have been limited to continental

65 scales (e.g. *9*) or are largely qualitative (e.g. *12*). Consequently, global patterns and magnitudes of

66 vegetation compositional change, which are important for understanding how biodiversity and

67 ecosystem dynamics have been shaped by climate change and early human activity, are poorly

68 understood.

69   In parallel, paleoecological studies have shown the high sensitivity of terrestrial ecosystems to

70 the climate changes accompanying and following the last deglaciation (ca. 20,000 to 8200 cal yr BP;

71 20 to 8.2 ka, **Figs. 1C,D**) (*12*, *13*). In temperate and boreal regions, forest expanded from glacial

72 refugia as temperatures rose and precipitation patterns shifted, with widespread leading-edge range

73 expansions and, for some taxa, trailing-edge range contractions (*14*). Novel ecosystems emerged in

74 response to novel climates and the late Pleistocene extinction of megaherbivores (*15*). Tropical and

75 subtropical ecosystems responded to rising temperatures linked to increasing greenhouse gases (**Fig.**

76 **1D**) and hydrological shifts driven by precessional controls on monsoons and the Intertropical

77 Convergence Zone (*16*). Consequently, during the Pleistocene-Holocene transition, tropical

78 ecosystems substantially changed in species composition and canopy structures across all elevations

79 (*17*), while millennial- and centennial-scale hydroclimate variability caused abrupt changes in global

80 vegetation during the Holocene (*18*).

81   Ecosystem responses to humans and climate change over long timescales can now be assessed

82 globally, thanks to the century-long expansion of a global network of fossil pollen sequences anchored

83 by increasingly precise radiocarbon chronologies (e.g. *19*), the building of open, community-curated

84 data resources (*20*), and the development of new rate-of-change techniques (*21*). Here, we assess the

85 global patterns and rates of vegetation change from the last deglaciation, through the Holocene and up

86 to the current Anthropocene, based on 1181 fossil pollen sequences from the Neotoma Paleoecology

87 Database (*20*) covering all continents except Antarctica (**Fig. 1, Data S1**). These analyses are based on

88 continentally harmonized taxonomies and updated Bayesian chronologies with age-depth model

89 uncertainties and an improved algorithm (R package *R-Ratepol*; *21*, *22*) for estimating Rates of

90 Change (RoC) for paleoecological time series. RoCs are calculated as the compositional dissimilarity

91 between consecutive time intervals (using the chi-squared coefficient) standardized by the length of

92 time between samples, therefore providing an indicator of compositional change per unit time. *R-*

93 *Ratepol* uses a moving-window approach (instead of the traditional calculation of dissimilarities

94 between individual levels), which minimizes artifactual alterations in RoC due to variations in sample

95 density and sedimentation rate (*21*). *R-Ratepol* also incorporates temporal uncertainty resulting from

96 age-depth modelling calculations via randomization (*21*, *22*). For each pollen sequence, we pooled

97 data into 500-yr time bins (see also our 250-yr sensitivity experiment in SM (*22*)) and calculated RoC

98 between bins to represent rate of compositional change through time. For each sequence, we also

99 identified time intervals with a large increase in rate of change, called 'peak points' (for more detailed

100 information see methods in SM (*22*)).

101 We analyze RoCs at the scale of continents and sub-continental clusters, defined by climatic

102 and geographic variables (*22*). For each continent and sub-continental region, we binned the RoC

103 scores per 500-yr time bins (with a 250-yr sensitivity experiment in SM (*22*)) and calculated the 95%

104 RoC quantile to highlight intervals and places with large vegetation changes while filtering out outliers

105 (see *22* for a comparison of the 95% quantile to median trends). Similarly, we calculated the

106 proportion of sequences with a peak point in each time bin. The clustering of peak points among

107 sequences indicates a synchronous period of abrupt vegetation change within a region. Generalized

108 Additive Models (GAMs) were fitted to all RoC and peak point curves to summarize trends and test

109 for significant accelerations (simultaneous confidence intervals of the first derivative differ from zero,

110 *22*).

111   We detect an unequivocal global acceleration of vegetation change during the late Holocene

112   (4.2–0 ka; **Fig. 2**). The estimated start of acceleration differs among continents and ranges from 4.6 to

113   3.1 ka (**Table S1**). This estimated start is well supported by the dense availability of samples during

114   the middle to late Holocene (**Fig. 1E**), but continental-scale estimates vary by ca. 500-1000 years (*22*).

115   For most continents, late Holocene RoCs are close to or exceed RoCs over the last 18 ka, with a

116   percent differential ranging from -6.3% to 22.2 % (**Fig. 2, Table S1**). Increases in RoC during the

117   Lateglacial and early Holocene can be linked to temperature and atmospheric CO_2 variations (**Figs.**

118   **1C,D**) and to hydrological variations. Rapid vegetation changes concentrate near to the onset of the

119   Holocene (11.7 ka) for most continents, expressed as a maximum in RoC or in peak points (**Fig. 2**). In

120   North America and Europe, RoCs reached maxima during the abrupt millennial-scale climate

121   oscillations characteristic of the North Atlantic and adjacent regions (ca. 15 to 11 ka), then

122   substantially declined during the early Holocene (**Fig. 2A, B**). The heightened rates of deglacial

123   vegetation change resembles the patterns of increased temperature variability in the North Atlantic and

124   elsewhere in the Northern Hemisphere that were driven by a combination of orbital forcing,

125   atmospheric greenhouse gas concentrations, meltwater pulses to the North Atlantic, and shifting

126   patterns of heat transport (*23*). In Asia, rapid but asynchronous change characterizes the Lateglacial

127   and deglaciation period, with a maximum in RoCs or a clustering of peak points between 10 and 8 ka

128   (**Fig. 2C**). In Latin America and Africa, RoCs also reach maxima between 10 and 8 ka, which can be

129   linked to altered monsoonal rainfall associated with declining Northern Hemisphere summer

130   insolation (*24*).

131   RoC patterns at subcontinental scales are consistent with known histories of climate change

132   and human land use. For example, in Eurasia, the western and northern European clusters show strong

133   peaks in the rate of vegetation change between 15 and 10 ka (**Figs. 3A,E**), consistent with the response

134   of vegetation to North Atlantic climate variations and the retreating Eurasian ice sheets (**Fig. 1C**). Late

135   Holocene rates of vegetation change are high across western and central Europe and particularly in

136   areas of high present and past agricultural activity (*10*). In Asia, high rates of vegetation change during

137   the early Holocene can be linked to post-glacial forest expansion in northern Asia (*25*) and to

138 millennial-scale variability in temperature and monsoonal rainfall in eastern Asia (*26*) (**Figs. 3C,D,I**).

139 Seven of ten Eurasian clusters show increased RoCs during the late Holocene.

140   In the Americas, vegetation RoCs vary by latitude and between Atlantic- and Pacific-adjacent

141 regions (**Fig. 4**). Eastern North America resembles western Europe in its high vegetation RoCs

142 between 15 and 10 ka, with a strong signal of synchronous vegetation change over the last millennium

143 (**Fig. 4G,H,I**). All North American regions show increased RoCs during the late Holocene except for

144 the high-latitude clusters. Driven by the topographic complexity of the Andes, vegetation responses in

145 the Neotropical highlands were highly variable and asynchronous (**Fig. 4D**) likely a combined effect

146 of changes in temperature, hydroclimate variability and atmospheric CO_2 (*27*, *28*). In the lowlands, a

147 peak in vegetation RoCs at 10 ka is likely due to hydrological variability linked to shifting monsoons

148 (**Fig. 4J**) (*27*). These large vegetation changes challenge the common myth of the 'stable' tropics and

149 suggest a strong sensitivity of the Neotropics to temperature, hydroclimate variability and orbital

150 precession during the early Holocene (*27*, *28*). In temperate South America, a period of synchronous

151 vegetation change in the Holocene (**Fig. 4E**) is asynchronous with warm Neotropical regions (**Fig.

152 4J**), likely due to varying climate modes influencing different parts of the continent (*29*). The late

153 Holocene acceleration of vegetation change is clearly manifested across most of the latitudinal

154 gradient of the Americas, except for the high northern latitudes, with the highest RoCs in coastal

155 western North America and eastern North America (**Fig. 4**).

156   The detection of globally accelerating rates of vegetation change during the late Holocene

157 provides a longer-term perspective to the well-documented increase in species turnover during the 20th

158 and 21st century (*6*). For terrestrial ecosystems at least, these recent increases in species turnover are

159 the continuation of a longer acceleration that began millennia ago (**Fig. 2**). Moreover, this work

160 suggests that contemporary communities and some current biodiversity trends may be partially due to

161 legacies of past land use or environmental forcing (*11*) in combination with the strong anthropogenic

162 imprint of the last decades. Hence, recent changes in biodiversity patterns represent only the most

163 recent interval of our used planet (*30*) that has been altered by millennia of changing environments and

164 human activities.

165　　　　　Our study has focused primarily on detecting patterns of rates of vegetation compositional

166　　　changes over the last 18,000 years and secondarily on attributing causes. This approach follows the

167　　　standard delineation in climate change research between detection studies that focus on establishing

168　　　the significance and fingerprints of observed climate trends (*31*) and attribution studies that explore

169　　　the potential causes of the observed events and patterns (*32*). Biodiversity research is now achieving

170　　　the capability for global detection analyses (*2*, *6*) across an increasingly broad range of timescales. The

171　　　next major frontier is to disentangle and attribute the contributions of climatic variability and

172　　　anthropogenic impacts to past vegetation changes. This attribution is challenged by the complex

173　　　interplay among climatic, anthropogenic, and vegetation dynamics that varies within and among

174　　　ecosystems, particularly at local to regional scales. For instance, in the Holocene in East Africa, land

175　　　cover changes over the last 6000 years were driven by multiple cultural and technological innovations

176　　　and by changes in rainfall amount and seasonality (*33*). In South America, Holocene climate

177　　　variability contributed to regime shifts in human demography and displacement, which in turn affected

178　　　ecosystems regionally (*34*). The worldwide spread of agricultural land-use over the last 3000 years

179　　　suggests intensified resource management (*8*), but was accompanied in some regions by significant

180　　　climate changes (*16*, *33*). Deglacial vegetation dynamics, although strongly climate-driven, were also

181　　　affected by global megaherbivore extinctions during the late Quaternary (*15*), that likely resulted from

182　　　synergistic anthropogenic and climatic drivers (*35*). These interactions argue against single-cause

183　　　attributions of rates of vegetation change.

184　　　　　A key next step is to integrate these paleovegetation sequences with other paleoclimatic and

185　　　archaeological records in order to better understand the past feedbacks among climate, ecosystems,

186　　　and humans (*3*, *10*, *13*, *36*), and the legacy effects of these past interactions on the trajectory of

187　　　contemporary ecosystems. Assembled networks of paleovegetation, paleoclimatic, and anthropogenic

188　　　records need to be harmonized and quality checked in order to do this attribution correctly and handle

189　　　the spatial variations in vegetation, climate, and human histories within and among continents (e.g.

190　　　*36*). Such an integration will also need carefully chosen numerical techniques to formally detect the

191　　　onset of detectable human influence in paleoenvironmental time series and the variation in timing

192 within and among ecosystems (*29*). Additionally, a higher density of paleoecological records is still

193 critically needed, especially in topographically rich regions such as the Himalayas and the Andes

194 where climate heterogeneity is highest and human activities span millennia.

195   Despite these complexities, it is well known that the mean global temperature increases during

196 the last deglaciation (ca. 6°C) were several times larger than those of the middle to late Holocene (ca.

197 1°C, *37*). Hence, a reasonable working inference is that the globally enhanced rates of vegetation

198 change over the last several thousand years were caused primarily by anthropogenic activities, while

199 vegetation changes during the late Pleistocene to early Holocene were driven primarily by changing

200 climates. If so, the magnitude and extent of late Holocene rates of vegetation change suggests that the

201 global transformation of the terrestrial biosphere by humans now resembles or exceeds in rate and

202 scope even the profound ecosystem transitions associated with the end of the last glacial period.

203 Moreover, the global ecosystem changes for this century may be greater yet, given current climate

204 commitments and given that the climate changes expected for higher-end emission scenarios are

205 similar in magnitude to those of the last deglaciation.

206

References and notes

1. B. J. McGill, M. Dornelas, N. J. Gotelli, A. E. Magurran, Trends Ecol. Evol. 30, 104–113 (2015).

2. M. Dornelas et al., Glob. Ecol. Biogeogr. 27, 760–786 (2018).

3. J. Woodbridge et al., J. Ecol. 109, 1396–1410 (2021).

4. E. C. Ellis, N. Ramankutty, Front. Ecol. Environ. 6, 439–447 (2008).

5. S. L. Pimm et al., Science 344, 1246752 (2014).

6. S. A. Blowes et al., Science 366, 339–345 (2019).

7. D. M. J. S. Bowman et al., J. Biogeogr. 38, 2223–2236 (2011).

8. L. Stephens et al., Science 365, 897–902 (2019).

9. T. Giesecke et al., Nat. Commun. 10, 5422 (2019).

10. L. Marquer et al., Quat. Sci. Rev. 171, 20–37 (2017).

11. C. N. H. McMichael, New Phytol. 229, 2492–2496 (2021).

12. C. Nolan et al., Science 361, 920–923 (2018).

13. D. A. Fordham et al., Science 369, eabc5654 (2020).

14. J. W. Williams, B. N. Shuman, T. Webb III, P. J. Bartlein, P. L. Leduc, Ecol. Monogr. 74, 309–334 (2004).

15. Y. Malhi et al., Proc. Natl. Acad. Sci. U.S.A. 113, 838–846 (2016).

16. F. E. Mayle, D. J. Beerling, W. D. Gosling, M. B. Bush, Phil. Trans. R. Soc. Lond. B 359, 499–514 (2004).

17. F. E. Mayle, M. J. Burn, M. Power, D. H. Urrego, in Past Climate Variability in South America and Surrounding Regions,

F. Vimeux, F. Sylvestre, M. Khodri, Eds., vol. 14 of Developments in Paleoenvironmental Research (Springer, 2009), pp. 89–112.

18. A. W. Seddon, M. Macias-Fauria, K. J. Willis, Holocene 25, 25–36 (2015).

19. S. G. A. Flantua et al., Rev. Palaeobot. Palynol. 223, 104–115 (2015).

20. J. W. Williams et al., Quat. Res. 89, 156–177 (2018).

21. O. Mottl et al., bioRxiv 2020.12.16.422943 [Preprint].

24 February 2021. https://doi.org/10.1101/2020.12.16.422943.

22. See supplementary materials online.

23. Z. Liu et al., Science 325, 310–314 (2009).

24. T. M. Shanahan et al., Nat. Geosci. 8, 140–144 (2015).

25. G. M. MacDonald, K. V. Kremenetski, D. W. Beilman, Phil. Trans. R. Soc. B 363, 2283–2299 (2008).

26. H. Zhang et al., Quaternary 2, 26 (2019).

241   27. V. F. Novello et al., Earth Planet. Sci. Lett. 524, 115717 (2019).

242   28. M. H. M. Groot et al., Clim. Past 7, 299–316 (2011).

243   29. S. G. A. Flantua et al., Clim. Past 12, 483–523 (2016).

244   30. E. C. Ellis et al., Proc. Natl. Acad. Sci. U.S.A. 110, 7978–7985 (2013).

245   31. PAGES 2k Consortium, Nat. Geosci. 6, 339–346 (2013).

246   32. K. E. Trenberth, J. T. Fasullo, T. G. Shepherd, Nat. Clim. Chang. 5, 725–730 (2015).

247   33. R. Marchant et al., Earth Sci. Rev. 178, 322–378 (2018).

248   34. P. Riris, M. Arroyo-Kalin, Sci. Rep. 9, 6850 (2019).

249   35. E. D. Lorenzen et al., Nature 479, 359–364 (2011).

250   36. A. Bevan et al., Proc. Natl. Acad. Sci. U.S.A. 114, E10524–E10531 (2017).

251   37. J. E. Tierney et al., Nature 584, 569–573 (2020).

252   38. North Greenland Ice Core Project members, Nature 431, 147–151 (2004).

253   39. E. Monnin et al., Science 291, 112–114 (2001).

254   40. O. Mottl, S. Flantua, HOPE-UIB-BIO/Global_RoC: First public release, version v1.0, Zenodo
255   (2021); http://doi.org/10.5281/zenodo.4650239.

256   41. S. G. A. Flantua et al., "Mottl et al. (2021, Science) Taxonomic harmonization tables for North
257   America, Latin America, Europe, Asia, Africa," Figshare, dataset (2021);
258   https://doi.org/10.6084/m9.figshare.13049735.

259

272   T.G., S.H., H.H., S.I., S.G.A.F, and J.W.W. led Neotoma data mobilization efforts. S.G.A.F. and

273   J.W.W. lead the writing. All authors contributed to the article and approved the submitted version.

274   **Competing interests**. The authors declare no competing interests. **Data and materials availability**:

275   All the data and R codes are publicly available at Zenodo (40) and at https://github.com/HOPE-UIB-

276   BIO/Global_RoC. Harmonization tables are available at Figshare (41).

277

278   **SUPPLEMENTARY MATERIALS**

279   Materials and Methods

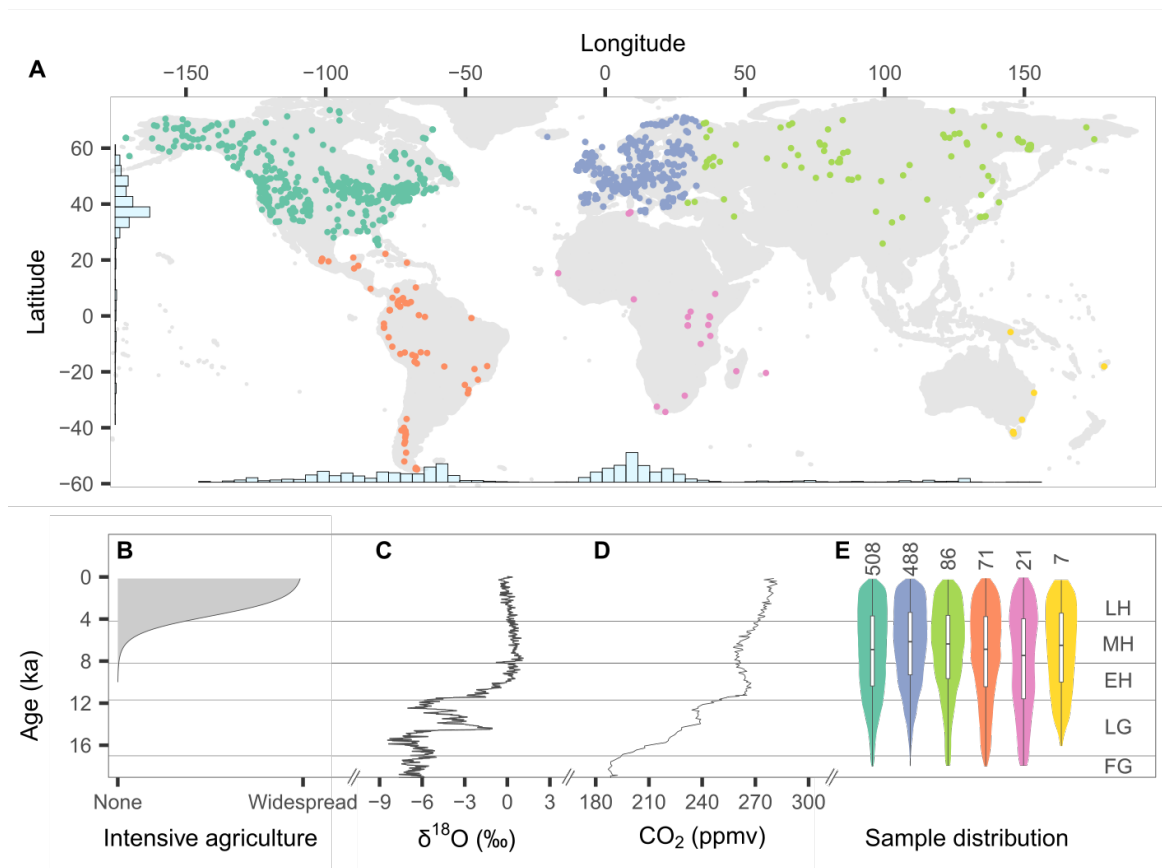280   Figs. S1-S7

281   Tables S1-S3

282   References (42-77)

283   Data S1

284

FIGURES AND TABLES

Figure 1 | Spatiotemporal distribution of the fossil pollen sequences analyzed here and climate and anthropogenic changes during the last 18.000 yr. A) Spatial distribution of used pollen sequences. Histograms indicate the frequency of sequences across longitude and latitude. B) Development of intensive agriculture based on archaeological expert elicitation (*8*). C) δ^{18}O, a temperature proxy, from the North Greenland Ice Core Project (NGRIP) (*38*). D) Atmospheric CO_2 concentration (ppmv; EPICA DOME C, *39*). E). The number of pollen sequences per continent (colors match panel A) and sample density over the studied period. FG: Full Glacial; LG: Lateglacial; EH: Early Holocene, MH: Middle Holocene, LH: Late Holocene.
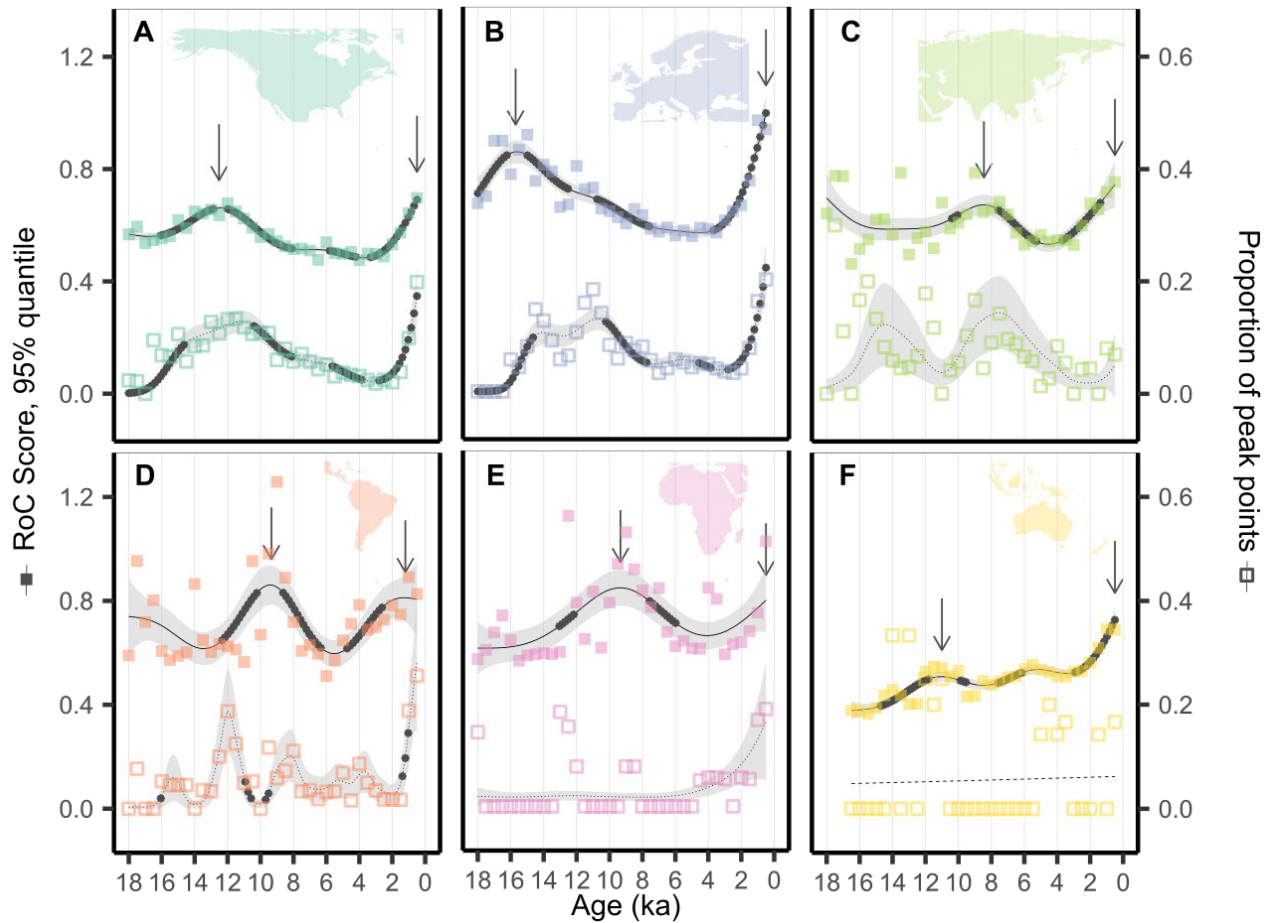
Figure 2 | Rate of Change (RoC) analyses by continent. The filled squares represent the upper 95%

quantile RoC score (left y-axis) per 500 yr time bin with the solid curve representing the

corresponding generalized additive model (GAM, *22*). High values indicate high rates of vegetation

change. Empty squares represent the proportion of peak points within each time bin (right y-axis) with

the corresponding GAM curve (dotted line). High values indicate a high synchrony in RoC among

sequences (*22*). When the relationship is not significant, the GAM line is shown as dashed and the

error envelope is absent. Black asterisks on the GAM curves identify periods of significant

acceleration in vegetation RoCs (i.e. where the derivative significantly differs from zero). Arrows

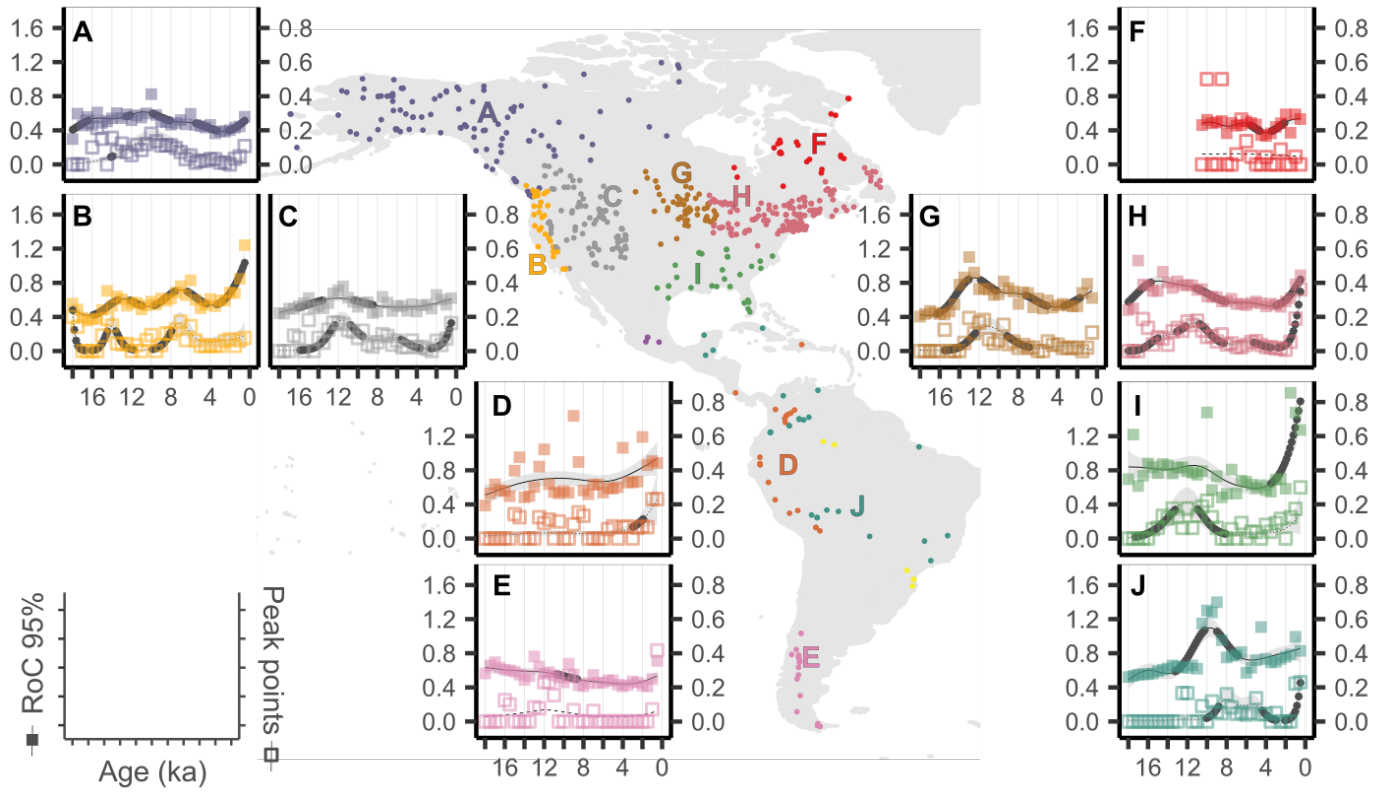indicate maximum RoC values for late Holocene and the Pleistocene-Holocene transition (**Table S1**).

308
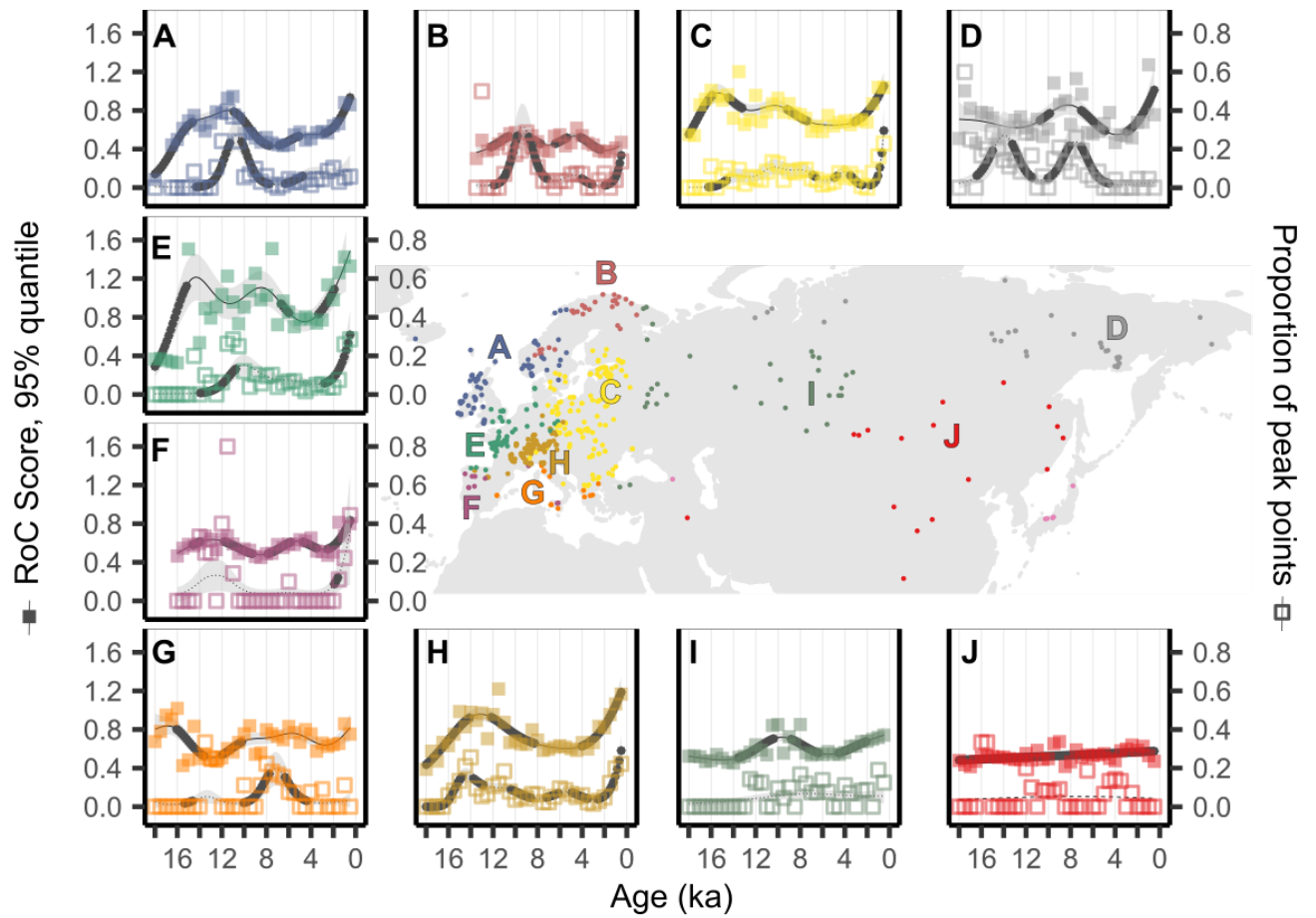
Figure 3 | Rates of Change (RoC) analyses by region across Eurasia. Figure design follows Figure

310   2.

311

Figure 4 | Rates of Change (RoC) analyses by region across the Americas. Figure design follows Figure 2.

Science

AAAS

1

2

3 ## Supplementary Materials for

4

5 ## Global acceleration in rates of vegetation change over the past 18,000 years

6

7 Ondrej Mottl[1]*†, Suzette G.A. Flantua[2]*†, Kuber P. Bhatta[1], Vivian A. Felde[2], Thomas Giesecke[3], Simon

8 Goring[4,5], Eric C. Grimm[6‡], Simon Haberle[7,8], Henry Hooghiemstra[9], Sarah Ivory[10], Petr Kuneš[11], Steffen

9 Wolters[12], Alistair W.R. Seddon[2], John W. Williams[4,5]

10

11 * Corresponding author. Email: ondrej.mottl@gmail.com, s.g.a.flantua@gmail.com

12 †Equal contribution. ‡Deceased.

13

14

15

16

17 **This PDF file includes:**

18
19 Materials and Methods
20 Figs. S1-S7
21 Tables S1-S3
22 Captions for Data S1

23
24 **Other Supplementary Materials for this manuscript include the following:**

25
26 Data S1

27

28

29

Material and methods

Data

We obtained fossil pollen data from the Neotoma Paleoecology Database using the *neotoma* R package V1.0 (*42*) on 26th May 2020, following data mobilization campaigns by Neotoma Data Stewards for the European Pollen Database, Latin American Pollen Database, African Pollen Database, North American Pollen Database, and other Neotoma Constituent Databases. These data mobilization projects have been supported by the Human On Planet Earth (HOPE) project (Advanced ERC grant 741413 to H.J.B. Birks) (https://www.uib.no/en/rg/EECRG/107501/hope), the Abrupt Change in Climate and Ecosystems (ACCEDE) project supported by the Belmont Forum (https://www.belmontforum.org/projects/), and on-going efforts by the Neotoma Paleoecology Database (https://www.neotomadb.org), supported by the Geoinformatics and EarthCube programs at NSF.

To develop age-depth models, we selected control point types (see the included types in **Table S3**), and calibrated the radiocarbon dates using the IntCal20, SHCal20 or mixed calibration curves (*43,44*). Calibration curves were assigned based on the geographical location of the records and the recommended boundaries provided by *44*. For each sequence with at least five chronological control points, we constructed an age-depth model using the *bchron* R package (*45*) to generate 1000 possible age estimates for all sample depths at the original sampling resolution of the original fossil pollen sequences. We used these 1000 draws to build posterior estimates of age uncertainty. We calculated the median age estimate for each sample depth to obtain the default age used in these analyses. All ages are expressed as in calibrated years before radiocarbon present (cal yr BP, where 0 yr BP = 1950 CE) or as kiloannum BP (ka), also in calibrated years before radiocarbon present.

53   We performed our analyses using the following delimitation of continents: North America, South America,

54   Europe, Africa, Asia and Oceania. The boundary between North America and Latin America was placed at

55   the border between the US and Mexico, while the boundary between Europe and Asia was placed at the

56   border between Russia and adjacent countries in Eastern Europe, including Finland, Belarus, Ukraine,

57   Bulgaria, and Greece. Taxa lists for North America, Latin America, Europe, Africa, and Asia were

58   harmonized to the taxonomically highest-precision pollen morphotypes identifiable by most palynologists.

59   The European harmonization was adjusted from Giesecke et al. 2019 (*9*) (Level = MHVar2,

60   http://www.europeanpollendatabase.net/data/downloads/image/EPD_P_VARS_high3.csv).   Taxonomic

61   harmonizations for other regions were developed for this paper specifically (North America) or as part of

62   the HOPE project (Asia, Latin America) or ACCEDE project (Africa; *46*) and are available at *41*. Data

63   from Oceania sequences were used at the original site-level taxonomic resolution. In each fossil pollen

64   sequence, we excluded 1) all samples that contained less than 150 pollen grain counts of terrestrial taxa, 2)

65   all samples with an age older than 18 ka, and 3) all samples for which the age has been extrapolated for

66   more than 3000 yr. We fully excluded marine sequences, all sequences spanning less than 5000 yr, and all

67   sequences with fewer than five samples.

68   <u>Identification of sub-continental regions by cluster analysis</u>

69   To study variations in rates of change in vegetation at sub-continental scales, we performed cluster analyses

70   based on geographical and contemporary climatic features of the fossil pollen sequences (**Figs. S4, S5**).

71   Geographical coordinates for sequences (longitude, latitude, elevation) were obtained from Neotoma, while

72   climate variables were obtained from CHELSA (*47*) based on climate normals for 1979–2013: a) Annual

73   Mean Temperature (BIO1; [°C*10]), b) Temperature Seasonality (BIO4; °C, standard deviation × 1000),

74   c) Precipitation of Driest Quarter (BIO17; [mm]), and d) Precipitation Seasonality (BIO15, [mm],

75   coefficient of variation).

76

77 We used the *NbClust* package (*48)* to identify sub-continental regions, 'clusters', for each continent and to

78 select an optimal number of clusters. Cluster analysis was performed separately for the six continents shown

79 in **Fig. 2**. Clusters were created using the seven previously mentioned geographic and climatic variables

80 (each of them standardized and centralized). We selected *McQuitty* as the clustering method and the

81 *Manhattan distance* to calculate distances among climate and geographic variables, because they result in

82 geographically homogeneous clusters, at a granularity appropriate for this global-scale synthesis. Note that

83 any clustering of continuous data will be sensitive to the choice of clustering method and distance metric

84 (*49)*, so the clusters shown here should be viewed as useful data-driven tools for understanding

85 subcontinental-scale variations in vegetation RoCs, but they are not definitive groupings. For this reason,

86 the major findings of this paper are primarily reported at the continental scale.

87

88 The minimum and maximum number of clusters were prescribed as 3 and 10, following a similar rationale

89 that at least three clusters were needed to assess subcontinental-scale variations, while more than 10

90 produced more granularity than needed for this global-scale analysis and risked clusters represented by few

91 or outlier datasets). We accepted all subcontinental clusters for display and analysis, except for North

92 America (**Fig. 4**), where the ten clusters originally identified led to an overly dense figure because North

93 and South America are shown simultaneously. For North America only, we did a post-hoc combination of

94 three of the original clusters, all in Alaska and Northwestern Canada into one cluster, to simplify the visual

95 presentation. The original *McQuitty* clustering for North America, i.e. prior to the post-hoc combination, is

96 available in **Fig. S7**.

97 <u>Rate of Change and Peak Point estimation</u>

98 We estimated the rate of change (RoC) score as well as the presence of a rapid change in taxonomic

99 composition (i.e. 'peak points') using the R-Ratepol package (*21*, *50*). RoC analysis estimates the

100 magnitude of compositional change per unit time, and so is a measure of community turnover that is related

101 to, but distinct from, most beta diversity metrics, which usually focus on species presence/absence data,

102   and may or may not follow a standard time step. Pollen data were smoothed using an age-weighted average,

103   in which samples were downweighted based on their temporal distance from the focus age (*51*). RoC was

104   calculated using the chi-squared coefficient metric of dissimilarity (*52*) and between consecutive time

105   intervals. To avoid artifactual variations in RoC caused by irregular temporal sampling resolution in the

106   original pollen sequences (*53*), Mottl et al. (*21*) developed a new approach that employs a variant of a

107   moving window, and is based on the following sequence: time bins of temporal width T are created, one

108   pollen sample is selected as representative of each bin, and RoC between bins is calculated. The brackets

109   of time bins (window) are then moved forward by a fixed time step (S), levels are selected again, and RoC

110   calculated for a new set of time bins. This is repeated five times while retaining all the results. For the

111   results shown in the main text, we set bin width (*T*) to 500 years (see section Sensitivity Analyses: Bin

112   Width), and time increment (*S*) to 100 years (i.e. five window shifts). *R-Ratepol* also incorporates

113   uncertainties in pollen sampling and uncertainties from age-depth models. In each randomization, 150

114   pollen grains are randomly sampled in each level and a single age sequence from age uncertainties is

115   randomly selected. The total number of randomizations is set to 1000. For each point, the median value of

116   all RoC scores from all randomizations is used as the final RoC score.

117

118   Peak points are defined as a significantly rapid increase in RoC score within individual sequences, and are

119   identified using a general additive model (GAM). For each RoC sequence, a GAM is fitted using variables

120   RoC and Age as $GAM(RoC \sim s(Age, k = 8))$. Residuals are calculated as the distance between the original

121   point-level value and the GAM fitted value, and the standard deviation of all residuals is tracked. A RoC

122   value is considered significantly large (i.e. a peak) if its residual is at least 2 standard deviations higher than

123   the fitted GAM. This identification of peak points provides a standard approach for comparison among

124   sequences and identification of time intervals characterized by increased RoCs across many sequences.

125

126   Some palynological indices of biodiversity and compositional RoC can be sensitive to variations in rare

127   pollen taxa, which in turn are often subject to higher uncertainty due to small counts (*52*, *54*, *55*). To reduce

128   the sensitivity of these analyses to the uncertainties associated with rare types, we made two analytical

129   decisions. First, we employed the chi-squared metric because it is in a class of signal-to-noise dissimilarity

130   metrics that is suitable for pollen counts with rare taxa (*52*). Previous studies have tested the skill of different

131   dissimilarity metrics when applied to fossil pollen data, e.g. for discriminating whether pollen assemblages

132   are from the same or different vegetation types (*54*, *55*). Signal-to-noise metrics, which includes the chi-

133   squared coefficient, have the highest skill because they draw signals from all pollen types while

134   upweighting the more abundant types, which are less subject to counting and identification uncertainties

135   than the rare taxa (*54*, *55*). In the context of this study, rare taxa can be expected to contribute to the RoCs

136   but will receive less weight than more abundant taxa. Second, the random sampling method described above

137   standardizes the pollen grains to a total of 150 pollen grains, reducing the number of rare taxa. Furthermore,

138   we performed an additional sensitivity test for the influence of rare taxa (<1% of pollen counts) on our rate

139   of change estimates (see below) to confirm that calculated rates of change were not sensitive to the high

140   uncertainties associated with rare taxa.

141   <u>Continental and regional RoC trends</u>

142   For each continent and sub-continental cluster, we pooled sequence-level RoC values into 500-yr bins (or,

143   for some sensitivity analyses, 250-yr bins) and calculated the 95% quantile score to focus on areas of large

144   vegetation changes while reducing sensitivity to outliers (see section below, *Summary Statistics: Behavior*

145   *and Sensitivity of the Median and 95th Quantile*). For each region, we also calculated the proportion of

146   peak points found per interval, relative to the distribution of samples across all sequences of a selected time

147   bin. We then constructed a GAM of the RoC values as $gam(RoC \sim s(time, k, \ bs = 'tp'))$ with a Tweedie

148   error distribution (with a self-estimated power parameter) and weights defined as $weights = 1 +$

149    $\left(\frac{the\ number\ of\ samples\ in\ time\ bin}{mean\ number\ of\ samples\ in\ all\ bins}\right)$. In order to avoid overfitting of the data while still reasonably

150   estimating the shape of the GAM curve, we followed the routine recommended within the *mgcv* package in

151   which a starting number of basis functions (k) was selected and the fit of the GAM to the data was checked,

152 using the *k.check* function from the *mgcv* package (*56, 57*). If a sufficient fit was reached, based on

153 randomly re-shuffled residuals (*58*), then the GAM model was complete. If not, k was increased in each

154 step until a sufficient fit was found. The choice of k effectively determines the degrees of freedom in the

155 GAM model, with higher k enabling a closer fit to data, while a too-high k will result in overfitting (*58*). In

156 this study the starting value of k was selected as 8 and each step increased by 4. To detect the significant

157 deviations of the GAM curve, we used the *fderiv* function from *gratia* package (*57*). Changes are considered

158 significant if the simultaneous confidence intervals of the first derivative of the GAM function differ from

159 zero (*56*). We followed a similar approach for the peak points, in which we constructed a GAM as

160 $gam(PeakProportion \sim s(time, k, bs = 'tp'))$ with beta error distribution. For the cluster-level GAMs,

161 we included only clusters with at least 10 fossil pollen sequences, to ensure that there were sufficient data

162 points for the RoC calculations to represent regional patterns instead of patterns driven by localized signals

163 in individual sequences.

164

165 To identify the timing of onset of the Late Holocene increases in RoC, we followed a simple algorithm in

166 which we began at the topmost time interval and then worked backwards in time to find the first point of

167 the continental RoC GAM curve that is significantly increasing (i.e. confidence intervals of the first

168 derivative of the GAM curve differ from zero).

169 Sensitivity Analyses: Bin Width

170 To test the sensitivity of our analyses to choice of bin width (T), we conducted sensitivity experiments with

171 bin widths of 500 years (**Fig. 2**) and 250 years (**Fig S2**; **Tables S1, S2**). We chose these bin widths based

172 upon several criteria. First, 500 years is a standard resolution for mapped syntheses of late Quaternary

173 pollen records that allows analysis of ecological responses to millennial-scale climate change during the

174 last deglaciation while also avoiding false temporal precision given radiocarbon dating uncertainties (*59–*

175 *61*). Second, the density of sequences and samples varies among time periods and continents and is highest

176 for the Holocene in Europe, eastern North America, and northwest South America (where a 250-year time

177 bin would be best supported by data) and lower for other time periods and regions.

178

179 The first-order temporal patterns of RoCs and peak points are insensitive to choice of bin width. Regardless

180 of choice of bin width, a Late Holocene acceleration is observed for most continents (**Figs. 2, S2**).

181 Moreover, Late Holocene rates of compositional change remain similar to or greater than rates of change

182 during the Pleistocene-Holocene transition. One question we aimed to address was whether the timing of

183 the Late Holocene acceleration might be attributable to choice of bin width and the degree to which recent

184 rapid changes in vegetation composition are smoothed backwards in time, e.g. in North America where

185 rates of land cover conversion have been particularly rapid following Euro-American arrival (*62*, *63*).

186 However, a comparison of the data points in **Fig. 2** (500-year bin) and **Fig. S2** (250-year bin) shows

187 remarkably little difference in timing of the late-Holocene acceleration for data-dense continents such as

188 North America and Europe. The biggest difference is that the plotted data are noisier when the 250-year

189 bins are employed, particularly for times and places where data densities are lower (**Fig. 1A,E**). As a result,

190 the GAMs often fit poorly to the data binned at 250-year timesteps (**Fig. S2**). Hence, we opted to base our

191 analyses on the data binned at 500-year timesteps, while retaining the 250-year binning for this sensitivity

192 analysis. We do not attempt here to formally attribute the Late Holocene acceleration in North America.

193 However, this acceleration likely is due to some combination of a growing anthropogenic footprint

194 associated with Early to Late Woodland cultures in eastern North America (*64–69*), Late Holocene climate

195 changes associated with declining summer insolation and unforced multi-centennial climate variability

196 (*70*), and the dramatic transformations of North American vegetation ca. 1650 to 1850 AD associated with

197 European arrival and intensified land use (*63*, *71*, *72*).

198 Sensitivity Analyses: Rare Taxa

199 To confirm that our results are not unduly affected by uncertainties in rare types, we ran our analyses with

200 a percentage threshold applied to all fossil pollen spectra, in which all taxa representing less than 1% of

201   total pollen terrestrial shrub, herb and tree pollen counts in each sequence were removed (**Fig. S3**). We

202   observe that the main patterns and conclusions remain consistent for all continents, though some periods of

203   high peak points are now more exaggerated (Africa) or smoothed (Oceania, Latin America) in lower data

204   density areas. Overall, the removal of rare taxa seems to strengthen the detection of synchronous periods

205   of abrupt vegetation change in all continents of the Northern Hemisphere and Latin America, with slightly

206   higher values in the proportion of peak points compared to **Figs. 2** and **S3**. However, overall trends remain

207   similar to the results based on the all-taxa dataset. The estimated timing of the Late Holocene increase in

208   RoC is not influenced by the inclusion of rare types (**Fig. S3**; **Table S3**). Hence, these analyses and

209   conclusions are generally robust to the inclusion or omission of rare taxa.

210

211   <u>Summary Statistics: Behavior and Sensitivity of the Median and 95th Quantile</u>

212   We chose the 95% quantile of RoC as a summary metric because initial data explorations indicated that the

213   mean and median were insensitive indicators of past vegetation change, particularly for the late-glacial and

214   Early Holocene (**Fig. S6**). All continents and metrics show the Late Holocene rise in vegetation RoCs, but

215   the median expression of vegetation RoCs is muted during earlier time intervals (**Fig. S6**), despite the large

216   known changes in vegetation during the last deglaciation (*12*, *17*, *73–77*). For any given time period, the

217   distribution of RoCs tends to be skewed, with many sequences showing moderate amounts of change, and

218   some sequences showing substantial changes (**Fig. S6**). This phenomenon is well illustrated in Europe and

219   North America, in which heightened rates of vegetation RoCs at the Pleistocene-Holocene transition at 11.7

220   ka are clearly visible in many individual sequences, yet the variations in the median are subtle. We attribute

221   this apparent insensitivity of the median to the increasing effects of temporal uncertainty for earlier time

222   periods. Because radiocarbon dates have a typical analytical uncertainty of several decades during the Late

223   Holocene, versus several centuries at the Pleistocene-Holocene transition, there is a stronger inter-sequence

224   blurring effect for earlier time intervals, which will be more strongly expressed in summary statistics that

225   rely upon the median and mean. Moreover, age estimates for the Late Holocene are anchored by a date of

226   high precision – the present – which has no counterpart across all the Lateglacial and Early Holocene

9

227   records. Hence, we view the 95% quantile as a more sensitive indicator of vegetation changes for earlier

228   time intervals. However, for areas and times with very low sequence density, such as Oceania, the 95%

229   quantile is likely to be overly sensitive to outlier records. Hence, interpretations in this paper focus on areas

230   and times of higher data density.

231

232   References

233   42. S. Goring, A. Dawson, G. L. Simpson, K. Ram, R. W. Graham, E. C. Grimm, J. W. Williams,
234   neotoma: A programmatic interface to the Neotoma paleoecological database. *Open Quat.* **1**, 2
235   (2015). doi:10.5334/oq.ab

236   43. P. J. Reimer, W. E. N. Austin, E. Bard, A. Bayliss, P. G. Blackwell, C. Bronk Ramsey, M. Butzin, H.
237   Cheng, R. L. Edwards, M. Friedrich, P. M. Grootes, T. P. Guilderson, I. Hajdas, T. J. Heaton, A.
238   G. Hogg, K. A. Hughen, B. Kromer, S. W. Manning, R. Muscheler, J. G. Palmer, C. Pearson, J.
239   van der Plicht, R. W. Reimer, D. A. Richards, E. M. Scott, J. R. Southon, C. S. M. Turney, L.
240   Wacker, F. Adolphi, U. Büntgen, M. Capano, S. M. Fahrni, A. Fogtmann-Schulz, R. Friedrich, P.
241   Köhler, S. Kudsk, F. Miyake, J. Olsen, F. Reinig, M. Sakamoto, A. Sookdeo, S. Talamo, The
242   IntCal20 northern hemisphere radiocarbon age calibration curve (0–55 cal kBP). *Radiocarbon* **62**,
243   725–757 (2020). doi:10.1017/RDC.2020.41

244   44. A. G. Hogg, T. J. Heaton, Q. Hua, J. G. Palmer, C. S. M. Turney, J. Southon, A. Bayliss, P. G.
245   Blackwell, G. Boswijk, C. Bronk Ramsey, C. Pearson, F. Petchey, P. Reimer, R. Reimer, L.
246   Wacker, SHCal20 southern hemisphere calibration, 0–55,000 years cal BP. *Radiocarbon* **62**,
247   759–778 (2020). doi:10.1017/RDC.2020.59

248   45. J. Haslett, A. Parnell, A simple monotone process with application to radiocarbon-dated depth
249   chronologies. *J. R. Stat. Soc. Ser. C Appl. Stat.* **57**, 399–418 (2008). doi:10.1111/j.1467-
250   9876.2008.00623.x

251   46. A. Vincens, A.-M. Lézine, G. Buchet, D. Lewden, A. Le Thomas, African pollen database inventory
252   of tree and shrub pollen types. *Rev. Palaeobot. Palynol.* **145**, 135–141 (2007).
253   doi:10.1016/j.revpalbo.2006.09.004

254   47. D. N. Karger, O. Conrad, J. Böhner, T. Kawohl, H. Kreft, R. W. Soria-Auza, N. E. Zimmermann, H.
255   P. Linder, M. Kessler, Climatologies at high resolution for the earth's land surface areas. *Sci.*
256   *Data* **4**, 170122 (2017). doi:10.1038/sdata.2017.122

257   48. M. Charrad, N. Ghazzali, V. Boiteau, A. Niknafs, NbClust: An R package for determining the
258   relevant number of clusters in a data set. *J. Stat. Softw.* **61**, 1–36 (2014).
259   doi:10.18637/jss.v061.i06

260   49. A. S. Shirkhorshidi, S. Aghabozorgi, T. Y. Wah, A comparison study on similarity and dissimilarity
261   measures in clustering continuous data. *PLOS ONE* **10**, e0144059 (2015).
262   doi:10.1371/journal.pone.0144059

263   50. O. Mottl, J.-A. Grytnes, A. W. Seddon, M. J. Steinbauer, K. P. Bhatta, V. A. Felde, S. G. A. Flantua,
264   H. J. B. Birks, R-Ratepol package, Github (2020); https://github.com/HOPE-UIB-BIO/R-
265   Ratepol-package.

266   51. L. Wilkinson, *The Grammar of Graphics* (Springer, ed. 2, 2005).

267   52. I. C. Prentice, Multidimensional scaling as a research tool in quaternary palynology: A review of
268   theory and methods. *Rev. Palaeobot. Palynol.* **31**, 71–104 (1980). doi:10.1016/0034-
269   6667(80)90023-8

270   53. A. F. Lotter, B. Ammann, M. Sturm, Rates of change and chronological problems during the late-
271   glacial period. *Clim. Dyn.* **6**, 233–239 (1992). doi:10.1007/BF00193536

272   54. J. T. Overpeck, T. Webb III, I. C. Prentice, Quantitative interpretation of fossil pollen spectra:
273   Dissimilarity coefficients and the method of modern analogs. *Quat. Res.* **23**, 87–108 (1985).
274   doi:10.1016/0033-5894(85)90074-2

275   55. D. G. Gavin, W. W. Oswald, E. R. Wahl, J. W. Williams, A statistical approach to evaluating distance
276   metrics and analog assignments for pollen records. *Quat. Res.* **60**, 356–367 (2003).
277   doi:10.1016/S0033-5894(03)00088-7

278   56. G. L. Simpson, Modelling palaeoecological time series using Generalised Additive Models. *Front.*
279   *Ecol. Evol.* **6**, 149 (2018). doi:10.3389/fevo.2018.00149

280   57. G. L. Simpson, H. Singmann, gratia: Graceful 'ggplot'-based graphics and other functions for GAMs
281   fitted using 'mgcv' (2019); https://rdrr.io/cran/gratia/.

282   58. S. N. Wood, *Generalized Additive Models: An Introduction with R* (Chapman and Hall/CRC Press,
283   ed. 2, 2017).

284   59. J. L. Blois, J. W. Williams, E. C. Grimm, S. T. Jackson, R. W. Graham, A methodological framework
285   for assessing and reducing temporal uncertainty in paleovegetation mapping from late-Quaternary
286   pollen records. *Quat. Sci. Rev.* **30**, 1926–1939 (2011). doi:10.1016/j.quascirev.2011.04.017

287   60. T. Giesecke, B. Davis, S. Brewer, W. Finsinger, S. Wolters, M. Blaauw, J.-L. de Beaulieu, H. Binney,
288   R. M. Fyfe, M.-J. Gaillard, G. Gil-Romera, W. O. van der Knaap, P. Kuneš, N. Kühl, J. F. N. van
289   Leeuwen, M. Leydet, A. F. Lotter, E. Ortu, M. Semmler, R. H. W. Bradshaw, Towards mapping
290   the late Quaternary vegetation change of Europe. *Veg. Hist. Archaeobot.* **23**, 75–86 (2014).
291   doi:10.1007/s00334-012-0390-y

292   61. S. G. A. Flantua, M. Blaauw, H. Hooghiemstra, Geochronological database and classification system
293   for age uncertainties in Neotropical pollen records. *Clim. Past* **12**, 387–414 (2016).
294   doi:10.5194/cp-12-387-2016

295   62. K. K. Goldewijk, A. Beusen, G. van Drecht, M. de Vos, The HYDE 3.1 spatially explicit database of
296   human-induced global land-use change over the past 12,000 years. *Glob. Ecol. Biogeogr.* **20**, 73–
297   86 (2011). doi:10.1111/j.1466-8238.2010.00587.x

298   63. J. H. McAndrews, in *Vegetation History*, B. Huntley, T. Webb, Eds., vol. 7 of *Handbook of*
299   *Vegetation Science* (Springer, 1988), pp. 673–697.

300   64. J. H. McAndrews, Late Quaternary vegetation history of Rice Lake, Ontario, and the McIntyre
301   archaeological site. *Archaeol. Surv. Can. Pap.* **26**, 161–189 (1984).

302   65. P. A. Delcourt, H. R. Delcourt, P. A. Cridlebaugh, J. Chapman, Holocene ethnobotanical and
303   paleoecological record of human impact on vegetation in the Little Tennessee River Valley,
304   Tennessee. *Quat. Res.* **25**, 330–349 (1986). doi:10.1016/0033-5894(86)90005-0

305   66. S. E. Munoz, K. Gajewski, Distinguishing prehistoric human influence on late-Holocene forests in
306   southern Ontario, Canada. *Holocene* **20**, 967–981 (2010). doi:10.1177/0959683610362815

307   67. S. E. Munoz, K. Gajewski, M. C. Peros, Synchronous environmental and cultural change in the
308   prehistory of the northeastern United States. *Proc. Natl. Acad. Sci. U.S.A.* **107**, 22008–22013
309   (2010). doi:10.1073/pnas.1005764107

11

310   68. W. W. Oswald, D. R. Foster, B. N. Shuman, E. S. Chilton, D. L. Doucette, D. L. Duranleau,
311   Conservation implications of limited Native American impacts in pre-contact New England. *Nat.*
312   *Sustain.* **3**, 241–246 (2020). doi:10.1038/s41893-019-0466-0

313   69. C. I. Roos, Scale in the study of Indigenous burning. *Nat. Sustain.* **3**, 898–899 (2020).
314   doi:10.1038/s41893-020-0579-5

315   70. J. Marsicek, B. N. Shuman, P. J. Bartlein, S. L. Shafer, S. Brewer, Reconciling divergent trends and
316   millennial variations in Holocene temperatures. *Nature* **554**, 92–96 (2018).
317   doi:10.1038/nature25464

318   71. N. Ramankutty, J. A. Foley, Estimating historical changes in land cover:North American croplands
319   from 1850 to 1992. *Glob. Ecol. Biogeogr.* **8**, 381–396 (1999). doi:10.1046/j.1365-
320   2699.1999.00141.x

321   72. T. M. Bonnicksen, America's ancient forests: From the ice age to the age of discovery. *Environ. Hist.*
322   **5**, 567–568 (2000). doi:10.2307/3985594

323   73. S. T. Jackson, R. S. Webb, K. H. Anderson, J. T. Overpeck, T. Webb III, J. W. Williams, B. C. S.
324   Hansen, Vegetation and environment in Eastern North America during the Last Glacial
325   Maximum. *Quat. Sci. Rev.* **19**, 489–508 (2000). doi:10.1016/S0277-3791(99)00093-1

326   74. T. Giesecke, S. Brewer, W. Finsinger, M. Leydet, R. H. W. Bradshaw, Patterns and dynamics of
327   European vegetation change over the last 15,000 years. *J. Biogeogr.* **44**, 1441–1456 (2017).
328   doi:10.1111/jbi.12974

329   75. H. Binney, M. Edwards, M. Macias-Fauria, A. Lozhkin, P. Anderson, J. O. Kaplan, A. Andreev, E.
330   Bezrukova, T. Blyakharchuk, V. Jankovska, I. Khazina, S. Krivonogov, K. Kremenetski, J. Nield,
331   E. Novenko, N. Ryabogina, N. Solovieva, K. Willis, V. Zernitskaya, Vegetation of Eurasia from
332   the last glacial maximum to present: Key biogeographic patterns. *Quat. Sci. Rev.* **157**, 80–97
333   (2017). doi:10.1016/j.quascirev.2016.11.022

334   76. L. Petherick, H. Bostock, T. J. Cohen, K. Fitzsimmons, J. Tibby, M.-S. Fletcher, P. Moss, J. Reeves,
335   S. Mooney, T. Barrows, J. Kemp, J. Jansen, G. Nanson, A. Dosseto, Climatic records over the
336   past 30 ka from temperate Australia – a synthesis from the Oz-INTIMATE workgroup. *Quat. Sci.*
337   *Rev.* **74**, 58–77 (2013). doi:10.1016/j.quascirev.2012.12.012

338   77. H. Wu, J. Guiot, S. Brewer, Z. Guo, Climatic changes in Eurasia and Africa at the last glacial
339   maximum and mid-Holocene: Reconstruction from pollen data using inverse vegetation
340   modelling. *Clim. Dyn.* **29**, 211–229 (2007). doi:10.1007/s00382-007-0231-3
341

Figures and tables

343   **Fig. S1**


344
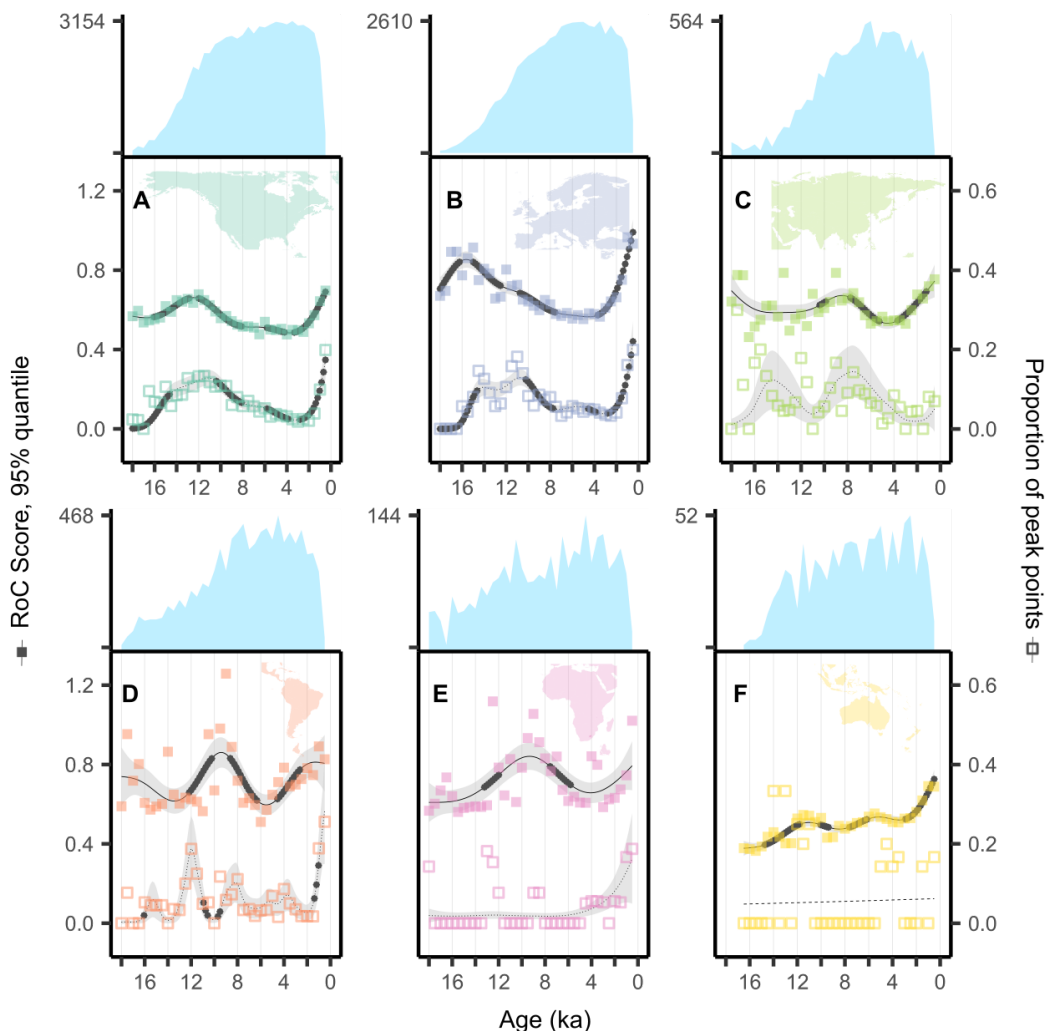
Fig. S1. Rates of Change (RoC) analyses and sample density by continent. Blue histograms indicate the number of samples per time interval. The rate-of-change and peak point squares and curves are identical to Fig. 2 and follow the same figure design. Solid line and filled squares represent the upper 95% quantile RoC score (bottom x-axis) where increased values indicate high change within the vegetation composition relative to time. The dotted line and empty squares represent the proportion of peak points within a time bin (*500 yr*) which is an indication of the degree of synchrony in RoC among sequences. When the relationship is not significant, the line is shown as dashed and the error envelope is not shown. Asterisks on the GAM curves identify where the curve significantly changes its course (i.e. where the derivative is significantly different from zero).
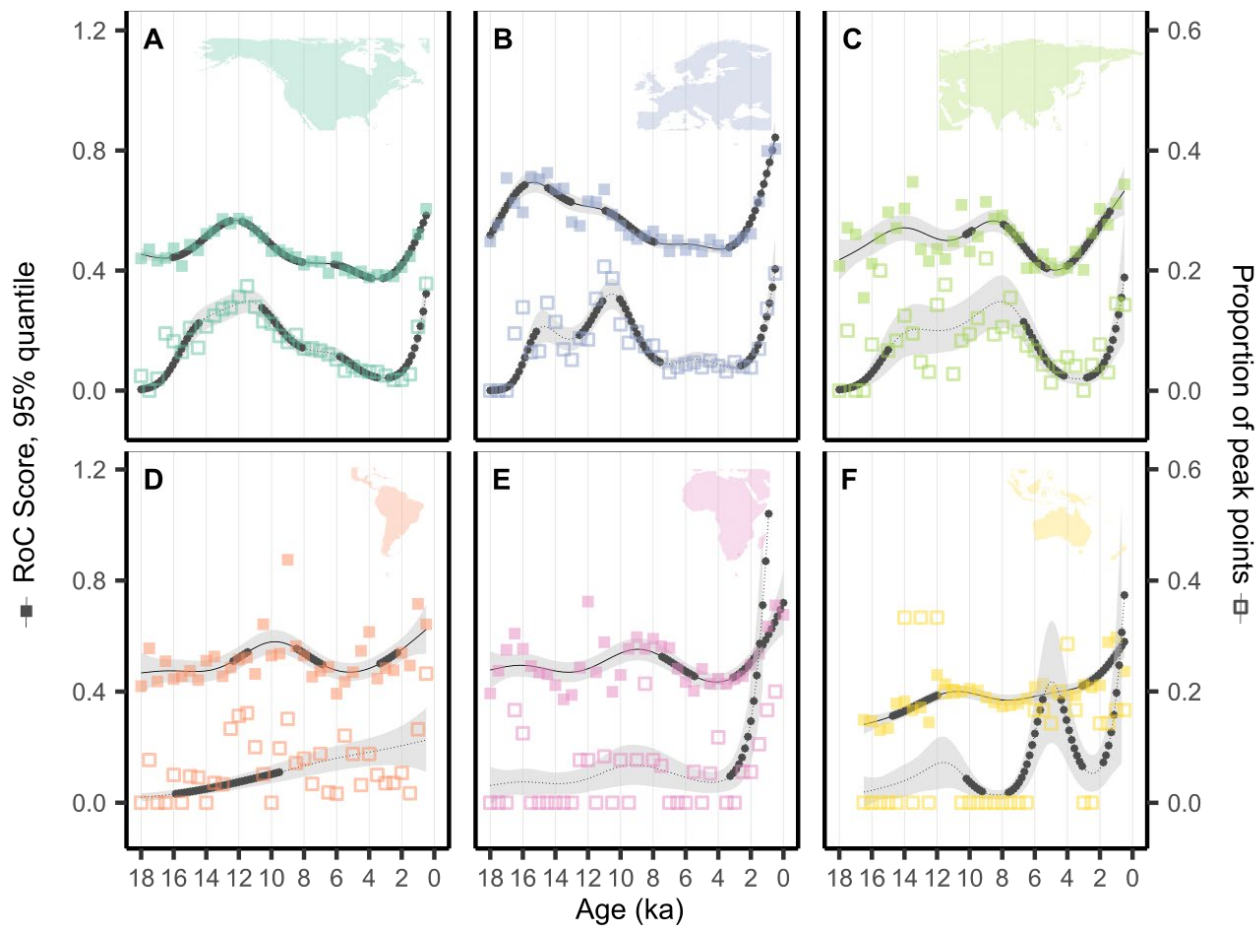
354

357
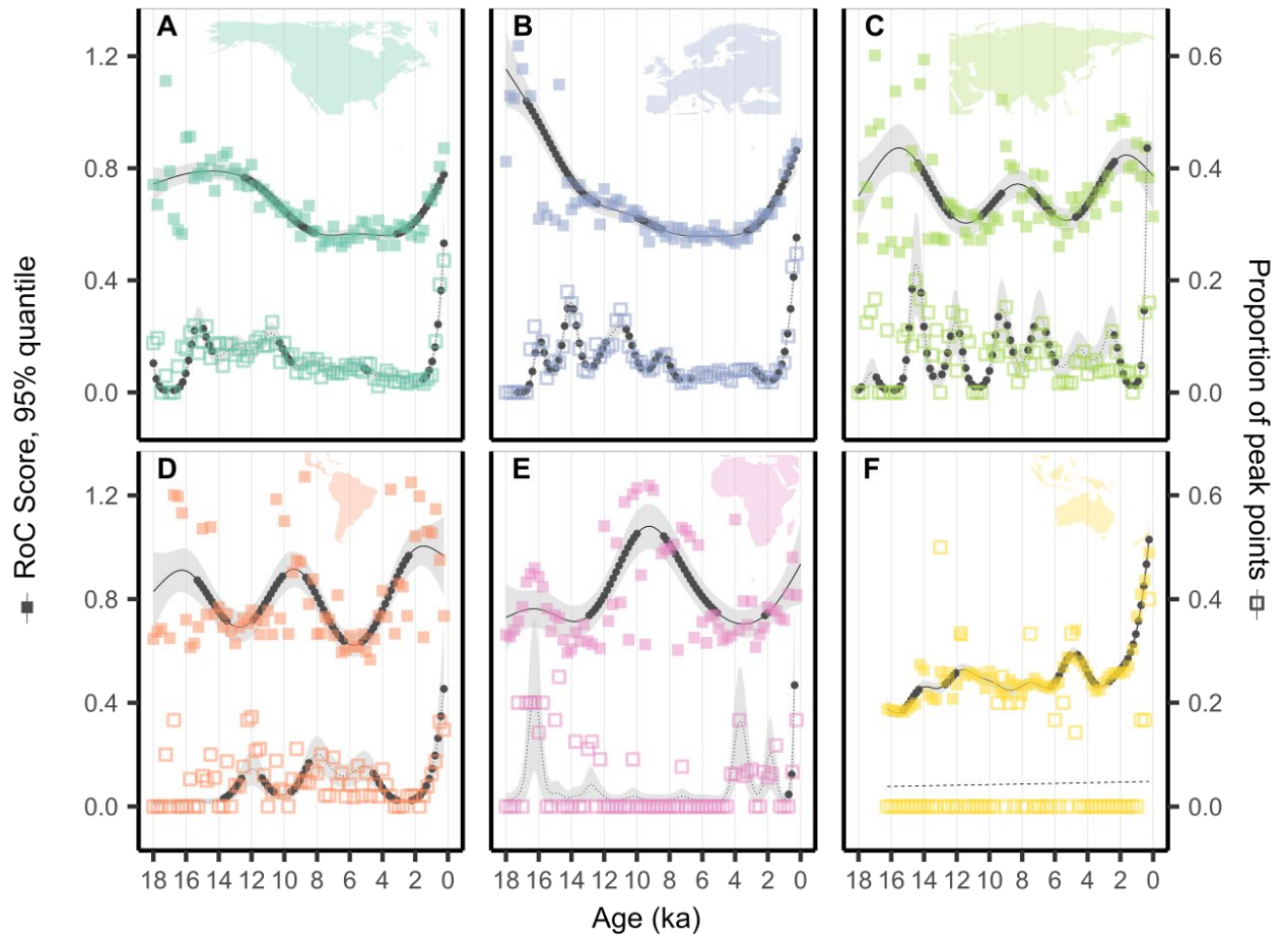
Fig. S2. Rates of Change (RoC) analyses by continent, for a sensitivity analysis with a temporal bin width of 250 years. The analyses shown here are identical to those shown in Figure 2, except that here the temporal bin width (T) is 250 years instead of 500 years. Figure design follows Fig. 2. See also Table S1.

361

364

Fig. S3. Rates of Change (RoC) analyses by continent based on a sensitivity analysis that excludes rare pollen taxa. The analyses shown here are identical to those shown in Figure 2, except that all taxa representing less than 1% of total pollen counts in a given sequence were removed from that sequence. Figure design follows Fig. 2.
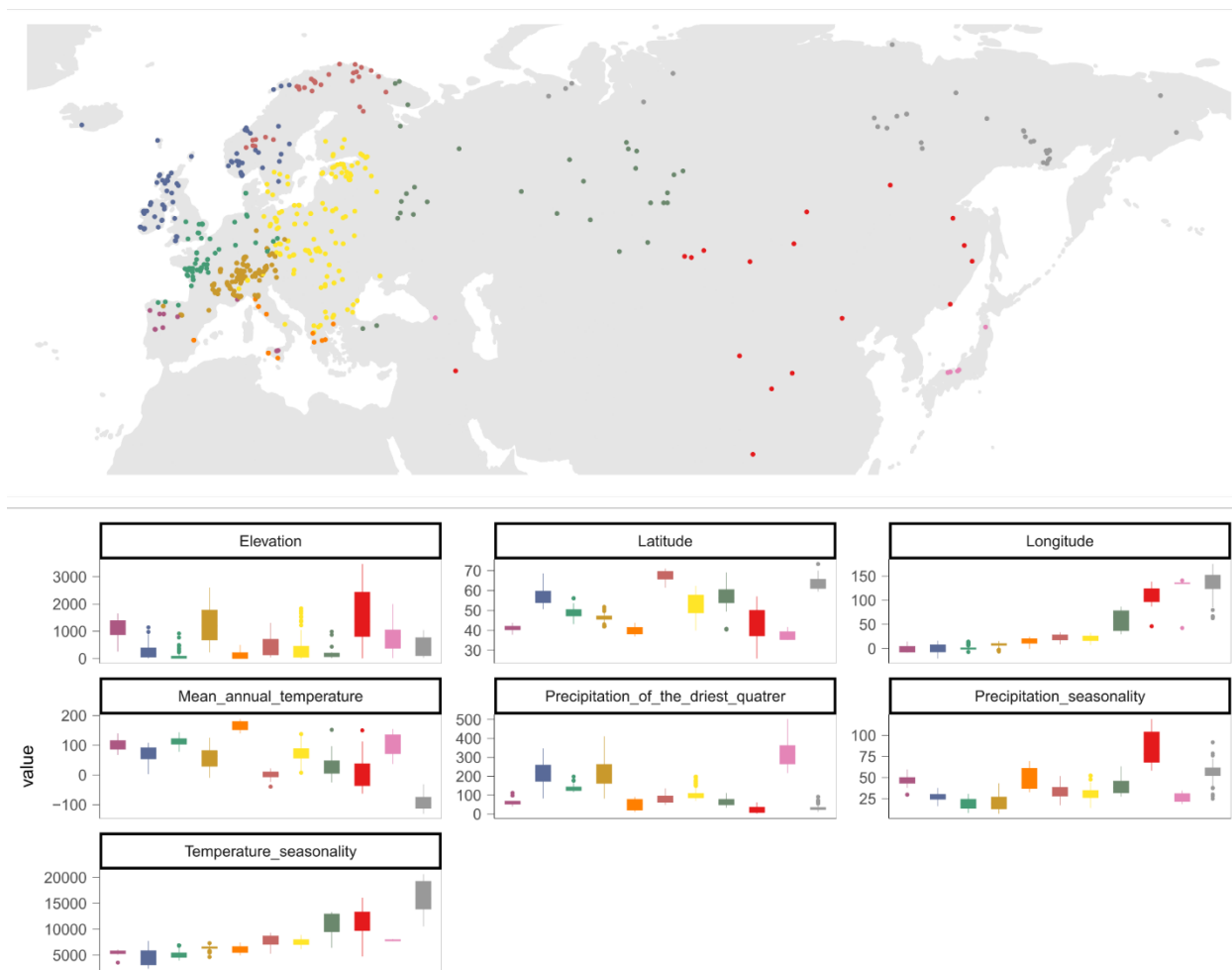
369

370

Fig. S4

Fig. S4. Environmental characterization of identified clusters for Eurasia. Fossil pollen sequences were assigned to clusters based on geographic and environmental properties (location, elevation, climate) at present. Colors from the boxplots correspond to the colors of the clusters displayed in the map. Elevation = meters above sea level, latitude = degrees north, longitude = degrees east, mean annual temperature [°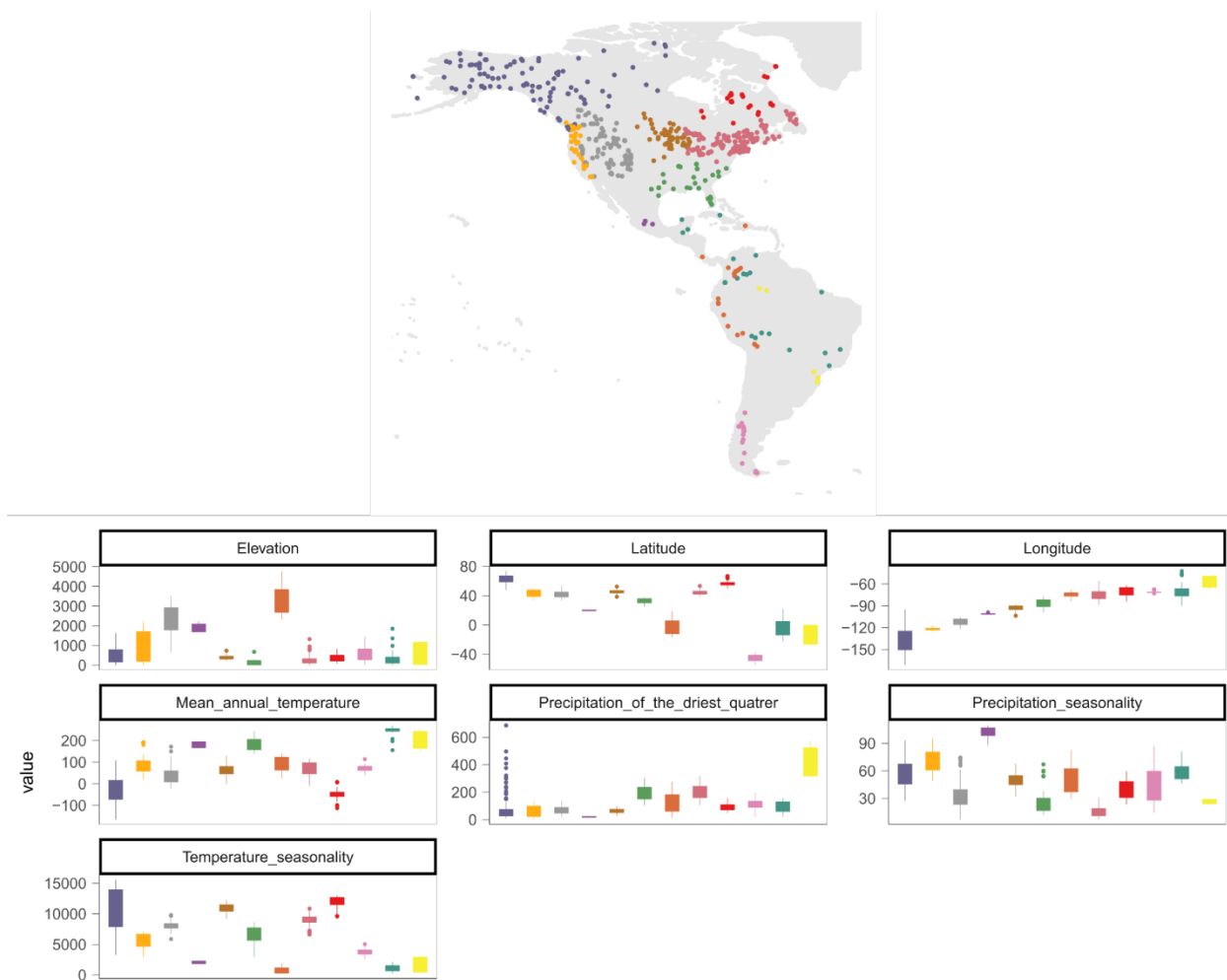C*10], total precipitation of the driest quarter (mm/quarter), precipitation seasonality (coefficient of variation), temperature seasonality (standard deviation *1000). See section on "Identification of sub-continental regions by cluster analysis" for more information about the methods used to identify clusters.
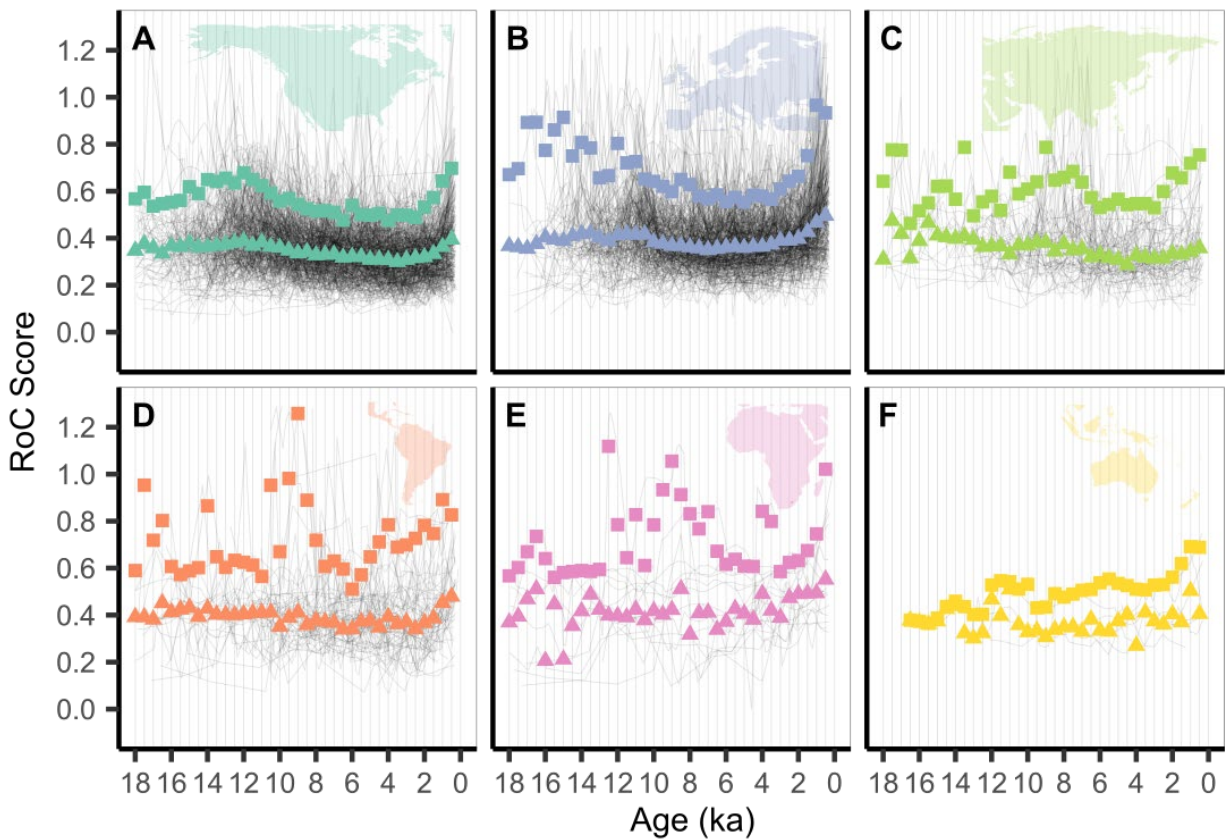
16

382 **Fig. S5**

383

384

385 **Fig. S5. Environmental variables for each cluster across the Americas**. Figure design follows Fig. S4.

386

Fig. S6
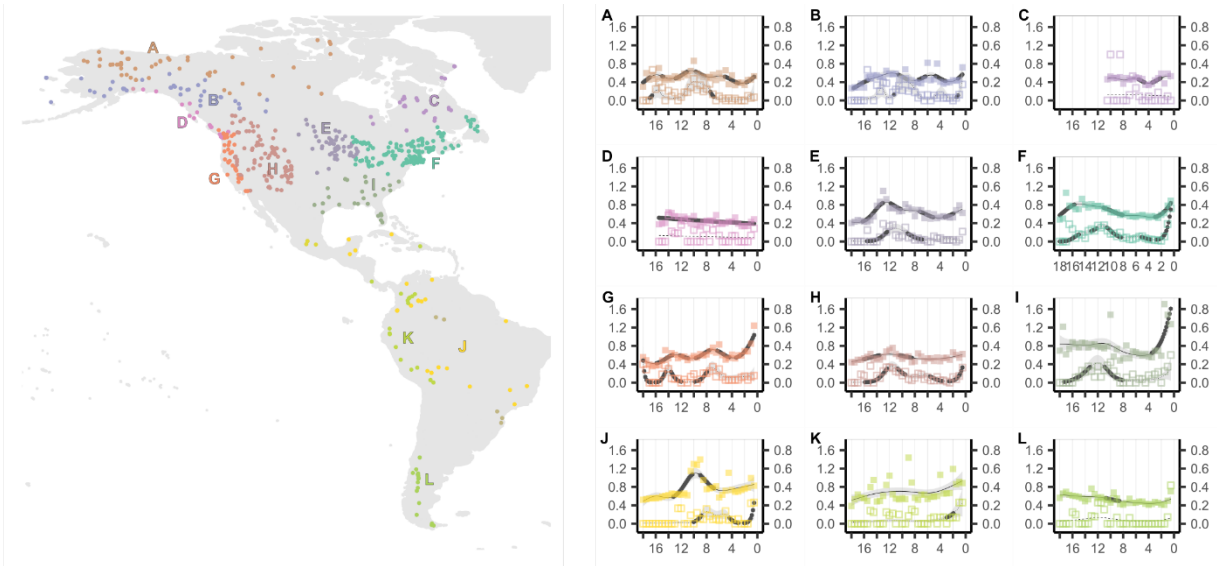
Fig. S6. Sequence-level Rates of Change (RoC) and summary statistics by continent, for both the median and 95th quantile. RoCs from individual sequences are shown as light gray lines. The 95th quantile is shown as filled squares and the median is shown as filled triangles. Color shading indicates continent, following the styles used in Figs 1, 2, and elsewhere.

394   **Fig. S7**

395

396   **Fig. S7. All identified clusters across the Americas with their corresponding Rates of Change (RoC)**

397   **analyses.** This figure displays all identified clusters across the Americas according to the performed

398   cluster analyses. For visualization purposes in Fig. 4, we merged clusters A, B, and D to one cluster A.

399

400

401

402   **Table S1**

Continent	Pleistocene-Holocene transition RoC maximum		Late Holocene RoC maximum		Late Holocene RoC increase (%)	Onset of Late Holocene acceleration (ka)	Explained variability of model
	Age (ka)	RoC score	Age (ka)	RoC score			
North America	12.5	0.66	0.5	0.69	4.4	3.3	0.93
Latin America	9.3	0.86	1.2	0.81	-6.2	4.6	0.43
Europe	15.7	0.85	0.5	0.99	14.1	3.7	0.89
Africa	9.3	0.84	0.5	0.79	-6.3	NA	0.37
Asia	8.5	0.67	0.5	0.75	10.7	3.7	0.47
Oceania	11	0.51	0.5	0.73	30.1	2.9	0.85

403

404   **Table S1. Summary table for GAM results shown in Fig. 2.** Columns 1 and 3 show the RoC scores for

405   the two maxima (indicated by arrows in Fig. 2) identified during the last 18 ka, while column 2 shows the

406   timing of the Lateglacial to Early Holocene maximum, and column 4 shows the timing of the Late Holocene

407   maximum in the fitted GAM. Column 5 shows the percent increase in RoC during the Late Holocene,

408   relative to its value at time of onset, while column 6 shows the estimated time of onset for the Late Holocene

409   increase. The identification of the onset of the Late Holocene increase is based upon the GAM detection

410   of statistically significant increases in rates of change, and specifically by first identifying the Late

411   Holocene accelerations found at the end of almost all records, then identifying the first-time interval in this

412   series with a statistically significant increase in vegetation rate of change. Column 7 shows the explained

413   variability of the GAM models shown in Fig. 2, which is expressed as a percentage of variability of fitted

414   model GAM. Calculations are based on 500 yr time bins. A lack of a significant increase in RoC values

415   during the last Holocene is indicated by NA.

416

417

418   20

419 **Table S2**

No.	Region	Onset of Late Holocene acceleration (ka)	Explained variability of model
1	Fig. 3A	2.8	0.86
2	Fig. 3B	6.4	0.63
3	Fig. 3C	3.2	0.64
4	Fig. 3D	3.0	0.39
5	Fig. 3E	3.3	0.49
6	Fig. 3F	2.5	0.67
7	Fig. 3G	NA	0.47
8	Fig. 3H	4.0	0.78
9	Fig. 3I	4.6	0.64
10	Fig. 3J	NA	0.17
11	Fig. 4A	2.1	0.64
12	Fig. 4B	3.3	0.76
13	Fig. 4C	NA	0.4
14	Fig. 4D	NA	0.22
15	Fig. 4E	NA	0.55
16	Fig. 4F	3.4	0.50
17	Fig. 4G	3.3	0.75
18	Fig. 4H	3.0	0.77
19	Fig. 4I	3.5	0.51
20	Fig. 4J	NA	0.63

420
421
422 **Table S2. Onset of the Late Holocene acceleration in rates of vegetation change among sub-**

423 **continental regions.** See detailed description Table S1.

424   **Table S3**

Control point type
"Annual laminations (varves)"
"Annual laminations (varves)/Sedimentation rate"
"Caesium-137"
"Collection date"
"Core top"
"Core top, estimated"
"Guess"
"Lead-210"
"Oxygen-18"
"Pb/Cs+AMS 14C"
"Radiocarbon"
"Radiocarbon, average of two or more dates"
"Radiocarbon, calibrated"
"Radiocarbon, calibrated from calendar years"
"Radiocarbon, calibrated, combined"
"Radiocarbon, infinite"
"Radiocarbon, reservoir correction"
"Radiocarbon, reservoir correction, calibrated"
"Section top"
"Tephra"

425   **Table S3. List of accepted chronological control point types.**

426

427

428

429

430   **Data S1.** (separate file)

431   **Metadata of fossil pollen datasets used in the analyses**. Dataset.id, sequence name, coordinates,

432   elevation, REGION (continent), References, CHELSA climate variables

433